EFFECT OF SI CONTENT ON IMPACT-ABRASIVE WEAR RESISTANCE OF AL2O3P/STEEL COMPOSITES PREPARED BY SQUEEZE CASTING

Dehong Lu, Haizhou Li, Bo Ren, Yehua Jiang

Faculty of Materials Science and Engineering, Kunming University of Science and Technology, 253 Xuefu Rd, Kunming, Yunnan, 650093, China

Keywords: Steel matrix composites, Si, Impact abrasive wear, Interfacial bonding strength, Wear mechanism

ABSTRACT

The objective of this work was to improve the impact-abrasive wear resistance of steel-based composites containing Al_2O_3 particulates (Al_2O_3p) through the use of squeeze casting and Si additions. In this case, Si powder ranging up to 25% of the Al_2O_3 content was added. Microstructures of the composites produced in this way were homogeneous in particle distribution and free from obvious defects. Composites were characterized by microscopy and with micro-indentation hardness tests of individual phases. The Si-free matrix contained only pearlite, but adding Si also produced ferrite. Impact-abrasion wear tests were performed using a hammer impacting on a rotating wheel that was flooded with quartz sand. The impact frequency was 80/min and the energy was of 2J. Adding Si obviously decreased the wear volume of the composites, and the minimum wear belonged to the 10% Si composite. The best wear-resistance can be attributed to two reasons: the relative higher hardness of the matrix and the strong interfacial bonding strength. The wear mechanism of the composites was abrasive wear when the Si content was less than 10%. At higher contents, it was a mixed mode of abrasive and delamination wear.

1 INTRODUCTION

As one of the commonest industrial problems, wear widely happens in mining, automotive, railroad and earth construction [1-3]. Nowadays, many studies have been focused on the development of wear-resistant materials, such as composite [4, 5], alloy steel [6, 7], and cemented carbide [8, 9]. Metal Matrix composites (MMCs), as a wear resistant material, are being increasingly used owing to their enhanced properties such as wear resistance combined with significant weight savings over unreinforced alloys. The commonly used metallic matrices include Al, Mg, Ti, Cu and their alloys [10, 11]. However, as is known to all, steel material cannot be replaced in engineering applications, especially the impact-abrasive wear conditions. Therefore, as the metallic matrix, steel material is vital to enhance wear resistance for Metal Matrix composites.

As metal matrix composites, steel based matrix composites reinforced with Al_2O_3 particulates (Al_2O_3p/steel composites) ideally combine the high hardness and wear resistance of Al_2O_3 ceramics with the ductility of steel metals, they show failure-tolerant behavior and therefore have the potential for a wide range of applications, especially the wear conditions [12-15]. However, at the present, the main limitations of Al_2O_3p/steel composites especially in wear related applications are their relatively low the strength and the hardness of the composites at room temperature. For example, S. Shamsuddin et al. [16] investigated a microhardness HV 80 for 25 weight percent Al_2O_3p/Fe-Cr steel composites. K. Lemster et al. [17] measured a bending strength 217 MPa for Al_2O_3p/X38CrMoV5-1 steel composites. This should be attributed to the weak interface bonding between Al_2O_3p and the steel matrix, because the wettability between pure Al_2O_3p and steel is very poor with a wetting angle of 150° [18, 19]. Therefore, the Al_2O_3p/steel composites often exhibit inferior wear-resistance, particularly in case of severe impact abrasive wear conditions. For example, in large ball mills, the liners made of Al_2O_3p/steel composite are easily dig out Al_2O_3p across the Al_2O_3p/steel interface due to the fact that abrasive particles intensely scratch and impact the liners.

In recent years, there have been some methods to improve the interfacial bonding strength in the Al_2O_3p/steel composites. K. Lemster et al. [20] fabricated Al_2O_3p/steel composites by pressureless infiltration method, in which Al_2O_3p preforms contained 20 wt.% Ti powder were infiltrated by the steel liquid at 1600 ºC for 24 h. E. Wang et al. [21] fabricated the Ni coating and the TiN coating on the surface of Al_2O_3p to improve the wettability between Al_2O_3 and the steel matrix. J. Feizabadi et al. [22] fabricated the nanostructure 304 stainless steel/Al_2O_3 composite by using self-propagating high temperature synthesis process to improve the wear properties of the composites. N.Travitzky et al. [23] obtained the Al_2O_3 reinforcement through reaction infiltration to fabricate the Al_2O_3p/Fe-Cr-Ni composites. However, problems still exist such as long fabrication period, low mechanical properties, high cost after all these research work. Therefore, it is urgent to seek efficient methods to improve the interfacial bonding and the mechanical properties for the Al_2O_3p/steel composites.

In this present work, the wear properties of Al_2O_3p/steel composites were improved through the use of squeeze casting and Si additions. The impact abrasive wear performance of the composites with different Si content was investigated. The wear mechanism was proposed, and the wear behavior of the composites was analyzed.

2 EXPERIMENTAL DETAILS

2.1 Materials

The experimental materials mainly included Si powder, Al_2O_3p and 5140 steel (C 0.44 wt.%, Cr 1.00 wt.%, Mn 0.60 wt.%, Si 0.30 wt.%, and the balanced Fe). The Al_2O_3p (from Saint-Gobain Ceramic Materials, Zhengzhou) were 99.75 weight percent in purity, 100~180μm in size. Si powder was 99.5 wt.% in purity and 180~250μm in size. The binder in the Al_2O_3p preform was sodium silicate ($Na_2O{\cdot}nSiO_2$) solution, in which n was 2.5.

2.2 Fabrication of composites

In this work, the composites were fabricated by squeeze casting technology [24], which consisted of three steps. Firstly, the Al_2O_3p preforms were prepared as follow. The Al_2O_3p, Si powder and the binder-sodium silicate solution were mixed in a ball mill for one hour. In this process, Si powder content was 5 wt.%, 10 wt.%, 15 wt.%, 20 wt.% and 25 wt.% of Al_2O_3p's mass, respectively and the binder-sodium silicate solution content was 3 wt.% of the total mass of Al_2O_3p and Si powder. Then the mixture was uniaxially pressed under 1MPa pressure to form the preform in a steel mold of 88 mm in diameter and 25 mm in height. Secondly, the demoulded preforms were heated up gradually from 20 ºC to 850 ºC at a heating rate of 5 ºC /min, during which preforms were held for an hour at 350 ºC. The heated preforms were placed rapidly at the bottom of a steel casting die which has a heat-insulation layer at the internal surface. Finally, the 5140 steel liquid infiltrated into the preforms to form the composites in the steel casting die by using squeeze casting. The squeeze casting process parameters included the pouring temperature 1580 ºC, the pressing time after pouring 10~15s, the pressure 79.5 MPa, and the pressure holding time 40s.

2.3 Microstructure and micro-hardness test

The standard metallographic specimens of the composites were cut from the castings. Then a standard method consisting of grinding, mechanical polishing and etching with 4% nitric acid alcohol was used for metallographic analysis. A Leica EZ4D optical microscope (OM) was applied to observe the microstructure of the specimens. A HITACHI S-3400N scanning electron microscope (SEM) was used to observe the worn surfaces. The Image-Pro Plus software was applied to calculate the volume fraction of the Al_2O_3p in the composites.

The Vickers hardness of the metal matrices in the composites was measured on polished samples using a micro-hardness tester (LEICAVMHT30M). The load was 200 g and the dwell time was 15s. Five micro-hardness values were measured for each matrix structure, and three of them were averaged after excluding maximum and minimum values.

2.4 The contact angle tests between steel containing Si and Al_2O_3p

To investigate the influence of the Si powder content in the preforms on the wettability, the contact angles between 5140 steel melt and Al_2O_3p were measured by the sessile drop method. Since only a few impurities in substrates can also affect the wetting, high purity Al_2O_3 substrates were used. The substrates had dimensions of 20 mm × 20 mm × 5 mm. The 3 mm × 3 mm × 3 mm 5140 steel specimens with different Si content were cut from the relative composites. Prior to measure the contact angles, those specimens were carefully cleaned in acetone with ultrasonic. The specimen was heated in a vacuum heating furnace. The contact angle was measured at 1873 K (1600 ºC) in a vacuum of less than 1.8×10^{-3} Pa. The sessile drop was photographed with a camera. The coordinates of twenty points on the outline of the droplet were measured on projections of the monochrome negatives and the contact angles were calculated by using the Laplace equation.

2.5 Impact abrasive wear tests

The impact abrasive wear tests were carried out on a pin-on-ring typed MLD-10 wear tester (produced by Taihua Machinery Co., Ltd.) at room temperature, as shown in Fig. 1. The upper specimen was the tested composites with the size of 10 mm × 10 mm × 30 mm. The lower specimen was a ring of 50 mm in diameter and 15 mm in thickness, made of 5140 steel with a hardness of 57 HRC. The abrasives were quartz particles, whose hardness (800~1200 HV) was lower than that of Al_2O_3p (1800~2200 HV) in the composites. This ensured that the reinforcement particles could resist the wear of abrasive particles. In order to identify the difference in the impact resistance of the composites with different Si content, the impact energy was determined as 2J. Other parameters included the hammer's impact frequency 80 times/min, the rotation speed of the lower specimen 180 r/min, the linear speed of rotating friction wheel 0.47 m/s, and the flow rate of the abrasives 5 kg/min. All specimens were first worn for half an hour to eliminate the test errors from the surface contact between the ring and pin, then formal tests for two hours and a half. Before and after each test, the specimens were ultrasonic-cleaned in alcohol and weighted using an electric balance with a precision of 0.0001mg to obtain the mass loss. The mass loss of each composite was the average value of three specimens.

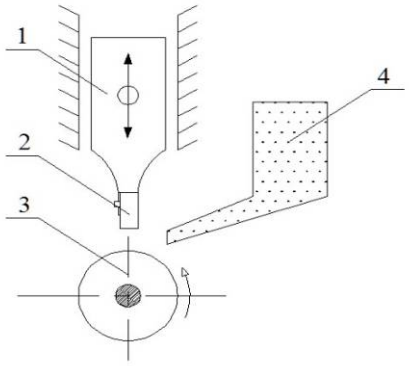

1-Dropping hammer; 2-Upper specimen 3-Lower specimen; 4-Quartz sand
Fig.1. Schematic diagram of MLD-10 tester

3 RESULTS AND DISCUSSIONS

3.1 Composites microstructure

Fig.2 shows the microstructure comparison of the composites without Si and with 15% Si, separately. There are some holes in the composite without Si (marked by circles in Fig. 2a), which are formed due to incomplete infiltration of the steel melt. However, there isn't any casting defect in the 15%Si composite, as shown in Fig.2 (c). Fig.2 (b) shows the matrix of the composite without Si consists of only pearlite. However, in Fig.2 (d), the matrix of the 15% Si composite is composed of black pearlite and white ferrite. Meanwhile, it is noteworthy that microstructure of the 15%Si composites is homogeneous in particle distribution.

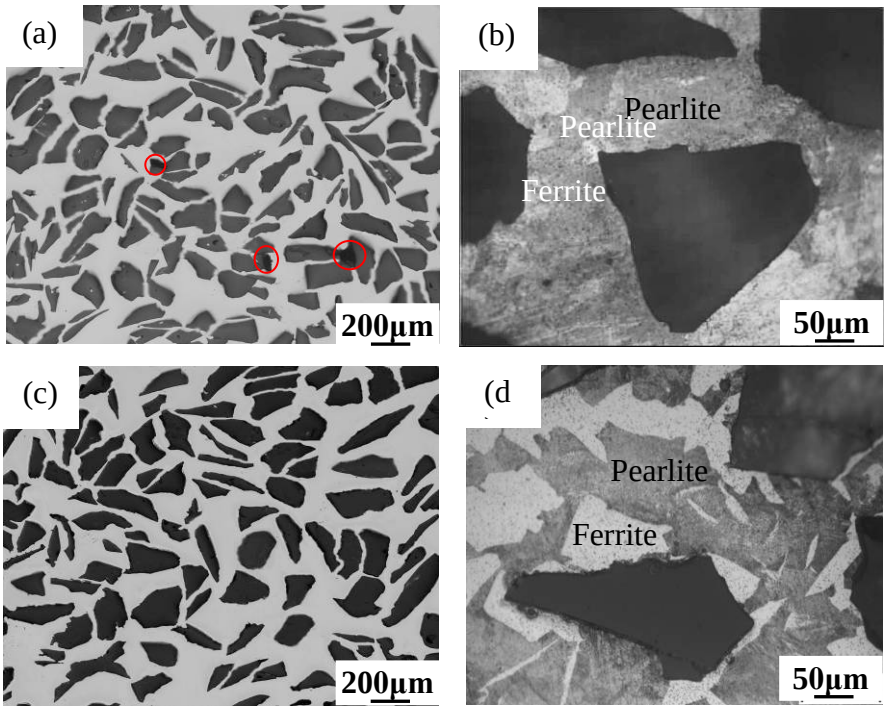

Fig. 2. Microstructure of (a) the composite without Si (not etched) and (b) the composite without Si (etched), (c) the 15% Si composite (not etched) and (d) the 15% Si composite (etched), by OM

3.2 Influence of Si content on wear performance of composites

The volume losses, instead of the mass losses, were applied to characterize the impact abrasive wear performance of the composites. This is mainly because there is a difference between the steel and Al_2O_3p in density. The volume loss of the composites was calculated as follow. Firstly, the mass losses were measured, as shown in Table 1.

Table 1 Mass loss of the composites

Si content / %	0	5	10	15	20	25
Mass loss / g	2.6924± 0.02	2.3531± 0.11	1.4230± 0.16	1.7983± 0.08	1.6934± 0.23	1.8803± 0.30

Subsequently, the density of the composites was calculated using the equation [25]:

$$\rho = \frac{m}{V} = \frac{1\times V_1 \times \rho_1 + 1\times V_2 \times \rho_2}{1} = V_1 \times \rho_1 + V_2 \times \rho_2 \quad (1)$$

Where V_1 is the volume fraction of the Al_2O_3p, ρ_1 is its density 3.98 g·cm^{-3}, V_2 is the volume fraction of the 5140 steel matrix, ρ_2 is its density 7.47 g·cm^{-3}. The volume fraction of Al_2O_3p was obtained according to measure the metallographic photo by using Image-Pro Plus 6.0 software. This method can ensure that the volume fraction is accurate and true. The result shows that the volume fraction of Al_2O_3p was 43.35%, 45.00%, 44.50%, 41.47%, 57.87% and 58.34%, respectively, as the Si content changed correspondingly from 0 wt.%,5 wt.%, 10 wt.%, 15 wt.%, 20 wt.% to 25 wt.% of Al_2O_3p. Moreover, M. R. Rosenberger et al. [26] in their investigations demonstrated that this theoretical density values match with the measured density values.

Finally, the volume losses of the composites were calculated by dividing mass loss with corresponding density. The result is shown in Table 2. Fig. 3 compares the volume losses of investigated composites. It shows that adding Si obviously decreased the wear volume of the composites. Fig. 3 also indicates that with the increase of Si content, the volume loss first decreased and then increased, reached the minimum wear at 10% Si composite.

Table 2 Volume loss of the composites

Si content/%	Density of composite/g·cm^{-3}	Volume loss/cm^3
0	5.96	0.45±0.01
5	5.90	0.39±0.02
10	5.92	0.24±0.02
15	6.02	0.29±0.02
20	5.45	0.31±0.04
25	5.43	0.35±0.04

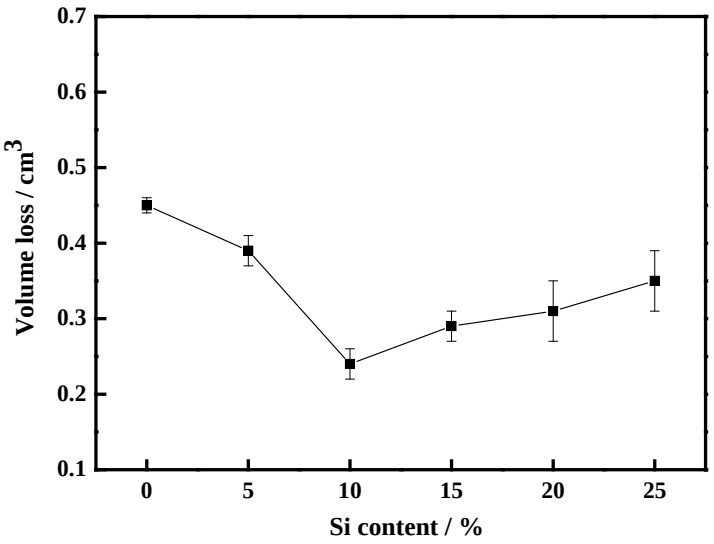

Fig.3. Relationship between volume loss and Si content

3.2.1 Influence of micro-hardness on wear performance of composites

Fig. 4 depicts the micro-hardness indentations of ferrite and pearlite in the steel matrix of the 20% Si composite. Fig. 5 shows the variation of Vickers hardness values of the metal matrix (ferrite, pearlite) with Si content. It is evident from Fig. 5 that the micro-hardness of the ferrite increased significantly when the Si content increased from 5% to 10%. This is mainly because the solid solution strengthening effect increased with the increasing Si content. However, when the Si content was above 10%, Si atoms started entering into pearlite. It gives rise to a decrease in the hardness of ferrite. As shown in Fig.5, when the Si content was above 15%, the hardness of pearlite decreased with the increasing Si content due to the increase of the volume fraction of the ferrite in the pearlite. In general, Si as an alloying element in steel, when added in small quantities, forms a solid solution with Fe, preferably ferrite [27]. Further, Calculating according to Fig. 6 shows that the volume fraction of ferrite in pearlite increased from 56.48%, 64.83% to 66.25%, as the Si content from 15 wt.%, 20 wt.% to 25 wt.%. This is attributed to the fact that the growth rate of the cementite in pearlite decreases due to the redistribution of Si between the cementite and ferrite [28].

It is well known that over the past decades, ferritic steels have not been widely used in applications requiring wear resistance. This could be contributed to the fact that the ferritic steels are relatively softer compared to other steels. However, the pearlite occurred in the soft ferritic matrix could improve hardness and abrasion resistance of steels matrix. Meanwhile, the abrasion resistance increased with the increasing volume fraction of pearlite [29]. Thus, the abrasion resistance mainly related to the hardness of pearlite. As mentioned above, when the Si content was higher than 10%, the volume fraction of ferrite in pearlite increased with the increasing Si content. This leads to the decrease of the pearlite hardness. For a soft matrix, large deformation and high density dislocations can be easily formed. Besides, a soft matrix could only bear low stress due to the low tensile strength.

It gives rise to the fact that the base material can be removed largely. Further, this result can be demonstrated by using the following formula [30]:

$$W_R = K\frac{P\varepsilon_{def}}{H\varepsilon_0} \tag{2}$$

Where W_R is the wear rate, H is the hardness, P is the applied load, ε_0 is the fracture strain of asperity, ε_{def} is the strain for asperity deformation and K is the wear coefficient. The above formula indicates that the wear rate of a material increases with decrease in hardness and fracture strain of the asperities. Thus, it is summarized that soft matrix would suffer more severe impact abrasive wear than hard matrix. It corresponds to the result of the wear experiments, as shown in Fig. 3.

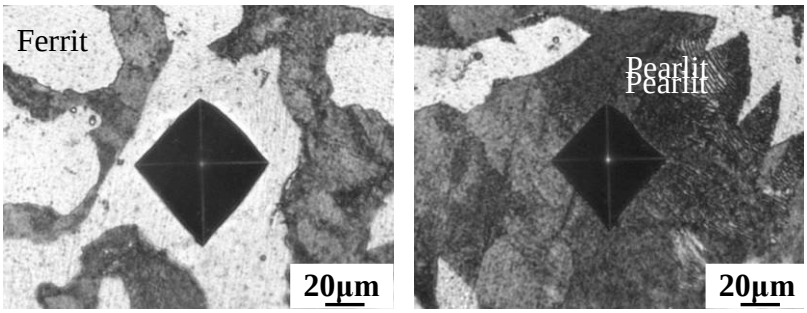

Fig. 4. Micro-hardness indentations in the matrix of 20%Si composite

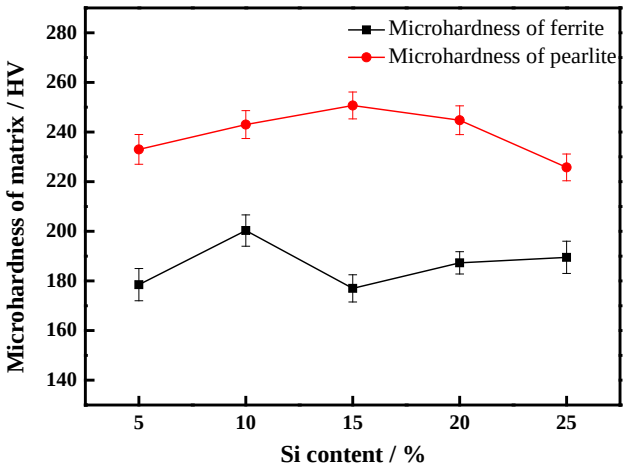

Fig. 5. Relationship between microhardness of the metal matrix and Si content

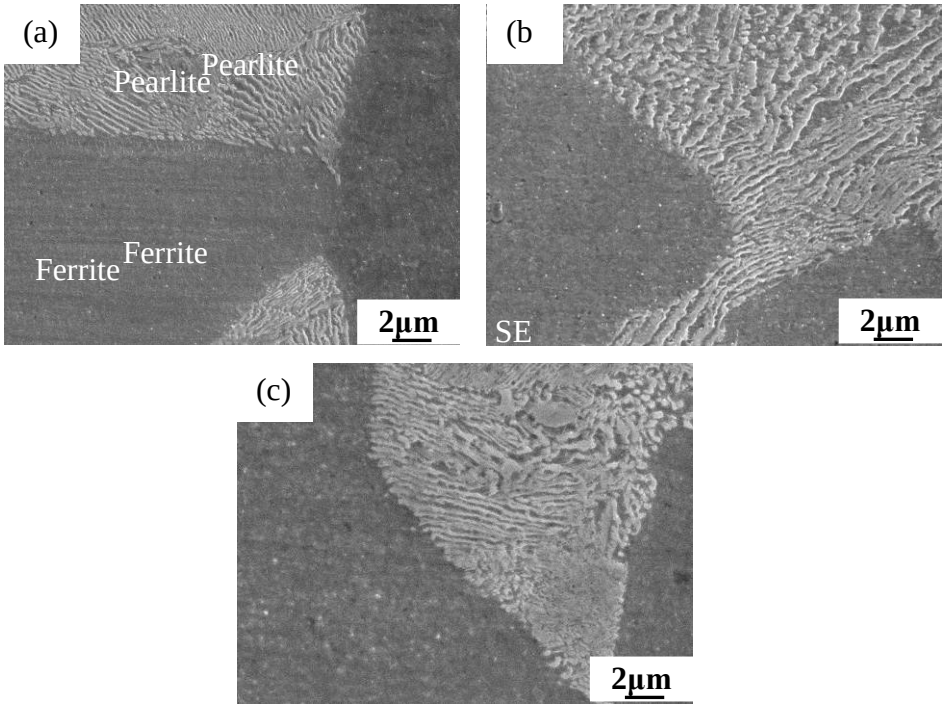

Fig.6 SEM observation of the metal matrix: (a) 15%Si composite; (b) 20%Si composite; (c) 25%Si composite

3.2.2 Influence of the contact angle between Al2O3 and steel on wear performance of composites

The contact angles between 5140 steel melt with Si and Al_2O_3p were measured by the sessile drop method. The results show that the contact angle was 125°, 118°, 114°, 111°, 107° and 105°, respectively, as the Si content changed correspondingly from 0 wt.%, 5 wt.%, 10 wt.%, 15 wt.%, 20 wt.% to 25 wt.% of Al_2O_3p, as shown in Fig. 7. This means that the contact angle decreased with the increasing Si content. Recent investigations by Cheng Zhang et al. [31] revealed that the enhancement of the bonding strength results from the formation of the metallurgical bonding at the interface as well as complete wettability between the reinforcements and the matrix. In essence, the metallurgical bonding between particles and the matrix material has a significant affect on the mechanical behavior of composites [32]. From the 5%Si curve of Fig. 7, we can see that the contact angle decreased remarkably from 144 to 118 degrees within the first 114s after a full melting. Afterwards, the contact angle value was kept at a stable value of 118 degrees (see Fig. 8) up to a time of 786 s. In this process, the decrease of contact angle is mainly because there was a $FeAl_2O_4$ phase in the interfacial cross section between the metal matrix and the Al_2O_3 substrates [18]. Therefore, it leads to the formation of metallurgical bonding at the interface. Meanwhile, the formation of metallurgical bonding is believed to be a important sign for the enhancement of the bonding strength.

On the other hand, good wettability can help to conquer the capillary pressure at the interfaces and to avoid the formation of interfacial flaws; both contribute to the interfacial adhesion. The relationship between work of the adhesion (W_{ad}) and the contact angle (θ) can be expressed as [33]:

$$W_{ad} = \gamma_{LV}(1+\cos\theta) \tag{3}$$

Where γ_{LV} is the surface tension of liquid-vapor phases. For a given solid surface, the solid-vapor γ_{LV} surface tension is expected to be constant. T. Laha [34] and R. E. Neuendorf [35] et al. presented a result that the lower the contact angle, the higher the work of adhesion and the better the bonding strength at the interface. Therefore, the Al_2O_3p/steel interfacial bonding strength and mechanical properties can be improved due to the decrease of the contact angle.

The wear behavior of particle reinforced composite depends on the type of interfacial bonding between the matrix and the particle reinforcement. When the Al_2O_3 particles are strongly bonded with the steel matrix, they protect the surface against sever destructive action of the abrasives. This is mainly because of the strong interfacial bond which plays a important role in transferring loads from

the matrix to the particles, resulting in less wear of the material [36]. The normal stresses generated at the poor interface easily exceed its bond strength [37]. It leads to the fact that in case of poor interfacial bonding, the interface offers site for crack nucleation and tends to pull out the particle from the wear surface. Therefore, the wear resistant of Al_2O_3p/steel can be improved due to the increase of interfacial bonding strength.

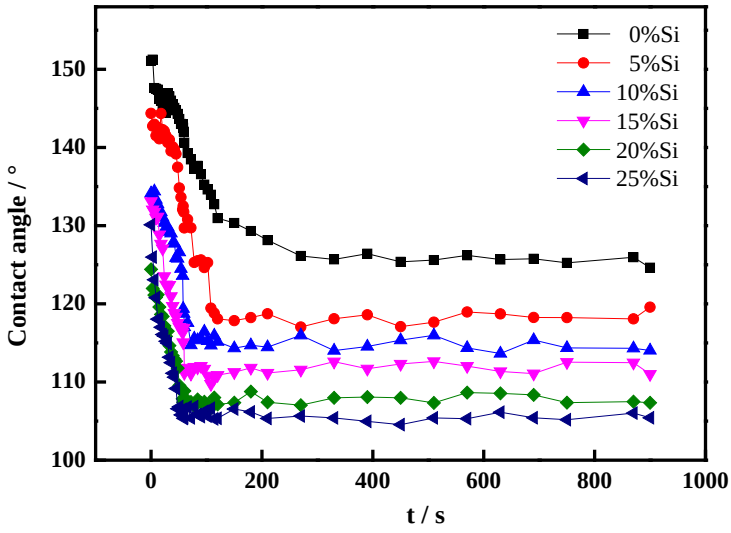

Fig. 7. The contact angles between the Al_2O_3 and the metal matrix with different Si content

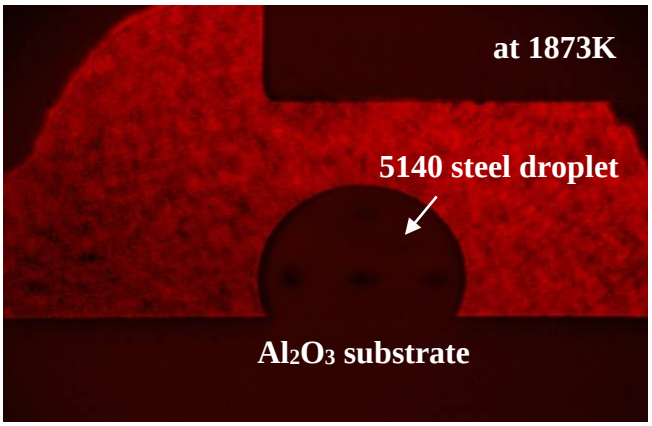

Fig. 8. Photograph showing the wettability (contact angles) of 5140 steel droplet on the Al_2O_3 substrate at 1873 K

3.3 Worn surfaces and sub-surfaces

The surfaces of the composites after 150 min wear are shown in Fig. 9. The features of the worn surfaces include furrow, fragmented Al_2O_3p, press-in particulates, plastic deformation, and sub-surface crack. Fig. 9(a) shows an abraded surface of the composite without adding Si. There are many wide, deep and parallel grooves which should be formed by microcutting of the abrasive particles, a result of the impact force of the hammer and shear force of the rotating wheel forcing abrasive into the metal matrix. Besides, there are press-in SiO_2 particulates and broken Al_2O_3p in the worn surface. The fragmentation of Al_2O_3p should be the result that brittle Al_2O_3p were suffered to strong impact load. Fig. 9(b) shows the worn surface of the 5%Si composite. From Fig. 9(b), it can be also obviously observed that severe grooves are the main feature, and exposed Al_2O_3p also can be seen in the worn surface. It indicates that the grooves were formed by microploughing [38] of the abrasive particles, and stopped by Al_2O_3p reinforcements. Fig. 9(c) indicates 10%Si composite is not worn heavily,

because there are little and shallower grooves and more exposed Al_2O_3p on the worn surface. Therefore, the wear mechanism is abrasive wear [39] when the Si content is less than 10%, and the wear volume decreases gradually with the increasing Si content.

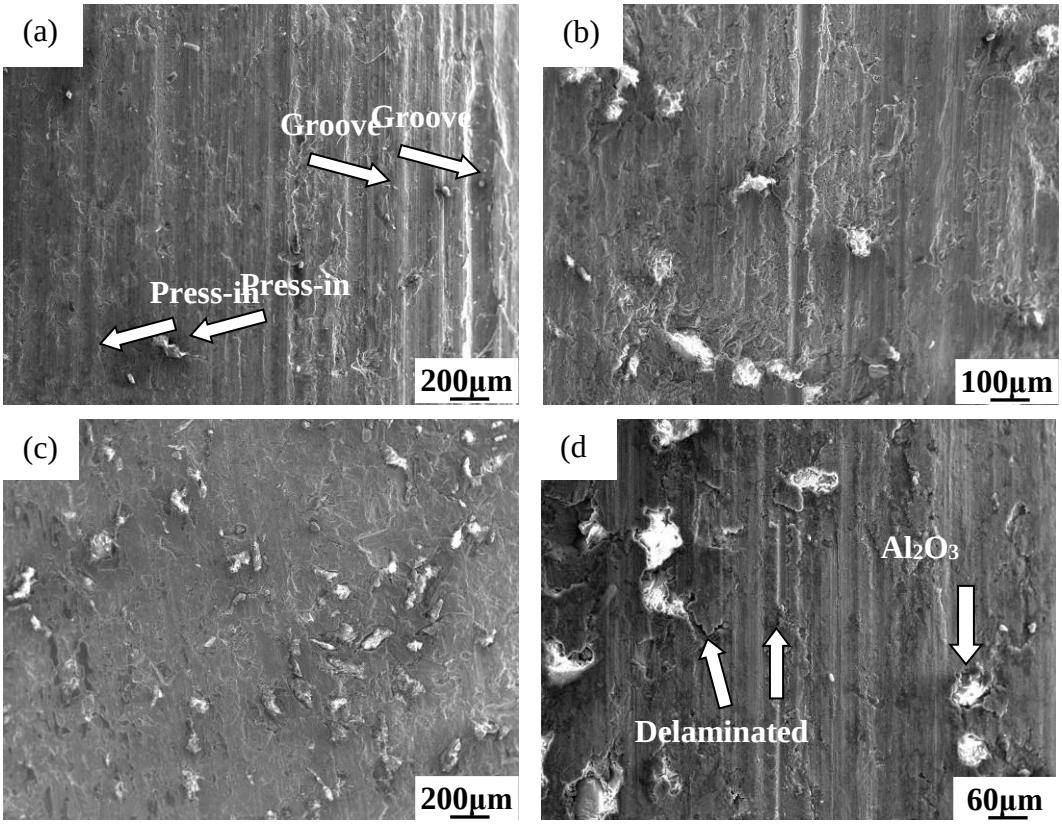

Fig. 9. SEM observation of worn surface of the composites: (a) 0%Si, (b) 5%Si, (c) 10%Si, (d) 25%Si.

Fig. 9(d) shows the worn surface of the 25%Si composite. It indicates that there are furrows formed by microploughing on the worn surface, and many cracks are present around exposed Al_2O_3p. The wear mechanism of abrasive wear should be also present. Moreover, it is evident from Fig. 10 (a) that a greatly oxidized layer occurs in the worn sub-surface. Fig. 10 (b) and (c) show that there is a large amount of O element and Fe element in the oxidized layer. Fig. 11 shows that there is a plastically deformed layer under the oxidation layer. All these indicates that a greatly oxidized deformation layer is formed on the worn surface of the composite due to intense plastic flow of the sub-surface materials under impact abrasive wear [40]. However, this intense plastic flow could be hindered by the Al_2O_3p. Therefore, as shown in Fig. 12, microcrack nucleation occurres at the interface between Al_2O_3p and matrix under the shear force of friction. Meanwhile, the cracks also propagate easily along the interface between the oxidization layer and below plastic deformation layer, as shown in Fig.11. The presence of the oxidization deformation layer and the cracks indicates that the wear mechanism of delamination exists for the 25% Si composite. Hence, the wear mechanism is a mixed mode of abrasive and delamination wear [41]. The schematic illustration of wear mechanism is shown in Fig. 13.

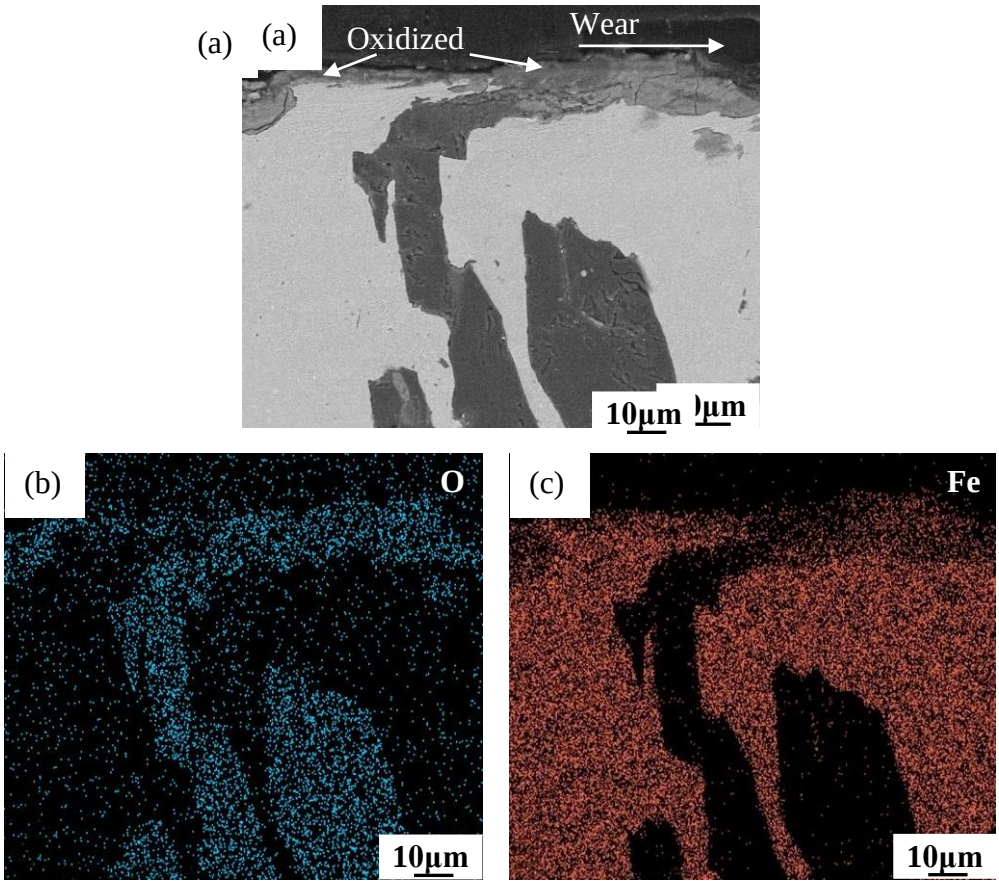

Fig. 10. the worn subsurface of 25%Si composite, (a) SEM image, (b) EDS of element O, (c) EDS of element Fe

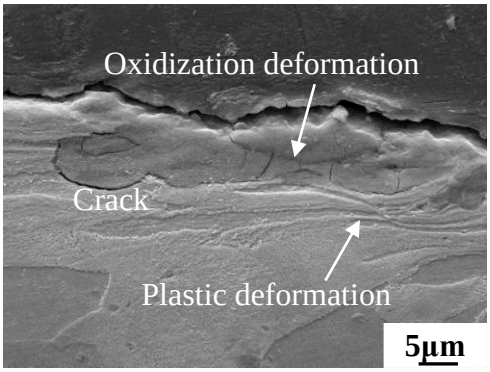

Fig. 11. SEM image of the subsurface of 25%Si composite.

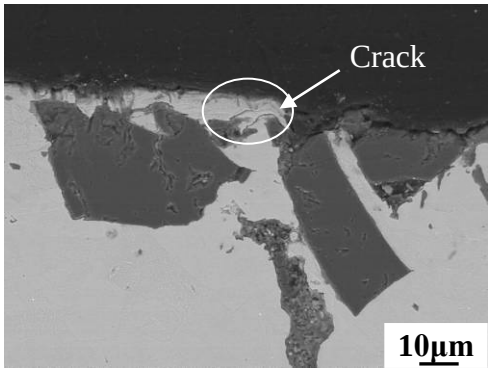

Fig. 12. Cracks in subsurface of 25%Si composite

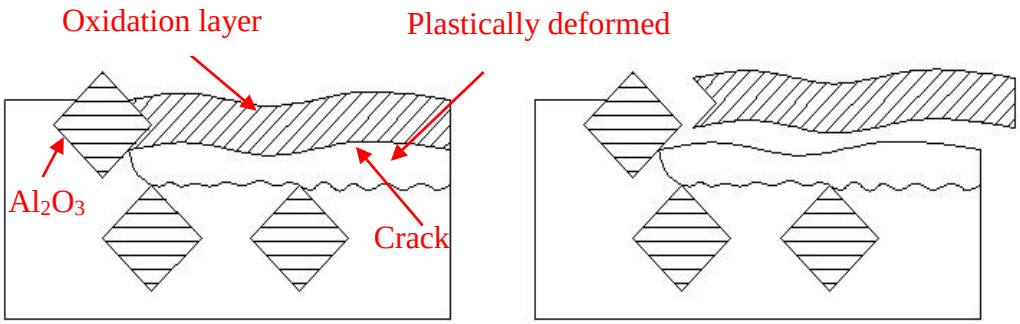

Fig. 13. The schematic illustration of delamination wear mechanism for the composites

3.4 Wear behavior of Al2O3p/steel composites

According to above analyses, the wear behavior of the composites can be described as follows:

The impact abrasive wear behavior of the Al_2O_3p/steel composites is likely controlled by a combination of the hardness of the metal matrix and the Al_2O_3p/steel interfacial bonding strength. As mentioned above, the wear mechanism is abrasive wear for the composites with Si less than 10%, so the dominant factors are the hardness of the metal matrix and the interfacial bonding strength. The composite without adding Si shows the lowest wear resistance, because the hardness of the matrix is the lowest which leads to its intense plastic flow, and the interfacial bonding strength is the weakest which causes spalling of Al_2O_3p from the matrix during wear. The wear behavior of the 5%Si composite is similar to the composite without Si. However, the 5%Si composite has the higher hardness of the metal matrix and interfacial bonding strength due to 5% Si adding. Therefore, the 5%Si composite has the higher wear resistance than the composite without Si.

The wear mechanism of the 10%Si composite is abrasive wear, and the dominant factors are the hardness of the metal matrix and the interfacial bonding strength. Besides, the volume fraction of Al_2O_3p can also affect the wear behavior of composites to some extent. In the wear experiment, the 10%Si composite exhibited best wear resistance. The reasons include three aspects. Firstly, its matrix has the highest hardness. Secondly, the stress triaxiality cannot be concentrated for the Al_2O_3p spacing in the 10%Si composite because the Al_2O_3p distributed uniformly in the matrix with the volume fraction about 44.5% [42]. Thirdly, the contact angle between the matrix and Al_2O_3p is lower than those composites with lower Si added, which indicates superior interfacial bonding. This gives rise to the fact that the reinforced hard Al_2O_3 particles protect the matrix surface against destructive action of the abrasive during wear process. Therefore, the grooves become shorter and shallower, because the grooves formed by microcutting are blocked by the exposed Al_2O_3p (see Fig.9(c)).

When the Si content is higher than 10%, the wear mechanism of the composites is a mixed mode of abrasive and delamination wear. In addition to the dominant factors, the degree of dispersion of Al_2O_3p also affects the wear behavior of the composites. On one hand, the matrix of the composites is easily microploughed due to lower hardness than the 10%Si composite. It leads to more wear. On the other hand, an increase in volume fraction of Al_2O_3p was found by increasing the Si content when Si content is higher than 10%. The increasing Al_2O_3p leads to a bad effect on the fracture toughness of MMCs especially with view to stress triaxiality [43] due to an decrease in the particle spacing and increase in Al_2O_3p/steel interface. This is mainly because the degree of Al_2O_3p clustering is expected to influence the wear performance by providing preferential sites for crack nucleation [16]. Thus, obvious interfacial cracks are present on the worn surface (see Fig. 9(d)). Subsequently, it leads to delamination of the oxidization layer. Therefore, the volume losses of the composites increase along with the increasing Si content when the Si content is higher than 10%.

4 CONCLUSIONS

This study investigated the effect of Si content added in the preforms on the wear performance of Al_2O_3p/steel composites fabricated by squeeze casting. The results are summarized as follows:

(1) The Si content in the preforms can strongly affect the microstructure and impact abrasive wear performance of Al_2O_3p/steel composites.

(2) The composite without Si adding contains only pearlite in the matrix, but those with Si adding contain both pearlite and ferrite.

(3) The composites with Si adding are less worn than the composite without Si adding. With the increase of Si content, the volume loss first decreases and then increases, reaches the minimum wear at 10% Si composite.

(4) The ferrite in the steel matrix of the 10%Si composite has the highest micro-hardness. However, the micro-hardness of the pearlite first increases and then decreases as the Si content increases, and reaches the peak value at 15%Si composite.

(5) With the increase of the added Si, the contact angles between steel and Al_2O_3p decreases.

(6) The wear mechanism of the composites is abrasive wear when the Si content is less than 10%, otherwise it is a mixed mode of abrasive and delamination wear. The wear behavior of the composites is controlled by a combination of the hardness of the metal matrix and the interfacial bonding strength.

ACKNOWLEDGEMENTS

This work was supported by the financial support of National Natural Science Foundation of China, Grant No. 51265019.

REFERENCES

[1] W. Wang, R. Song, S. Peng, Z. Pei, Multiphase steel with improved impact-abrasive wear resistance in comparison with conventional Hadfield steel, Materials & Design 105 (2016) 96-105.

[2] S.G. Peng, R.B. Song, T. Sun, F.Q. Yang, P. Deng, C.J. Wu, Surface failure behavior of 70Mn martensite steel under abrasive impact wear, Wear s 362–363 (2016) 129-134.

[3] C. Wang, X. Li, Y. Chang, S. Han, H. Dong, Comparison of three-body impact abrasive wear behaviors for quenching–partitioning–tempering and quenching–tempering 20Si2Ni3 steels, Wear s 362–363 (2016) 121-128.

[4] A. Lekatou, A.E. Karantzalis, A. Evangelou, V. Gousia, G. Kaptay, Z. Gácsi, P. Baumli, A. Simon, Aluminium reinforced by WC and TiC nanoparticles (ex-situ) and aluminide particles (in-situ): Microstructure, wear and corrosion behaviour, Materials & Design (1980-2015) 65 (2015) 1121-1135.

[5] K. Ji, Y. Xu, J. Zhang, J. Chen, Z. Dai, Foamed-metal-reinforced composites: Tribological behavior of foamed copper filled with epoxy–matrix polymer, Materials & Design 61(9) (2014) 109-116.

[6] M. Lindroos, M. Apostol, V. Heino, K. Valtonen, A. Laukkanen, K. Holmberg, V.T. Kuokkala, The Deformation, Strain Hardening, and Wear Behavior of Chromium-Alloyed Hadfield Steel in Abrasive and Impact Conditions, Tribology Letters 57(3) (2015) 1-11.

[7] M. Lindroos, V. Ratia, M. Apostol, K. Valtonen, A. Laukkanen, W. Molnar, K. Holmberg, V.T. Kuokkala, The effect of impact conditions on the wear and deformation behavior of wear resistant steels, Wear 328- 329 (2015) 197-205.

[8] W.M.D. Silva, M.P. Suarez, A.R. Machado, H.L. Costa, Effect of laser surface modification on the micro-abrasive wear resistance of coated cemented carbide tools, Wear 302(1–2) (2013) 1230-1240.

[9] Y. Xing, J. Deng, X. Feng, S. Yu, Effect of laser surface texturing on Si3N4/TiC ceramic sliding against steel under dry friction, Materials & Design 52(24) (2013) 234–245.

[10] R. Yamanoğlu, E. Karakulak, A. Zeren, M. Zeren, Effect of heat treatment on the tribological properties of Al–Cu–Mg/nanoSiC composites, Materials & Design 49(3) (2013) 820-825.

[11] S.L. Pramod, A.K.P. Rao, B.S. Murty, S.R. Bakshi, Effect of Sc addition on the microstructure and wear properties of A356 alloy and A356–TiB_2 in situ composite, Materials & Design 78 (2015) 85-94.

[12] A. Seupel, R. Eckner, A. Burgold, M. Kuna, L. Krüger, Experimental characterization and damage modeling of a particle reinforced TWIP-steel matrix composite, Materials Science & Engineering A 662 (2016) 342-355.

[13] D. Wittig, C.G. Aneziris, T. Graule, J. Kuebler, Mechanical properties of three-dimensional interconnected alumina/steel metal matrix composites, Journal of Materials Science 44(2) (2009) 572-579.

[14] X.H. Wang, M. Zhang, B.S. Du, Fabrication In Situ TiB_2 –TiC–Al_2O_3 Multiple Ceramic Particles Reinforced Fe-Based Composite Coatings by Gas Tungsten Arc Welding, Tribology Letters 41(1) (2011) 171-176.

[15] I.J. Shon, T.W. Kim, J.M. Doh, J.K. Yoon, S.W. Park, I.Y. Ko, Mechanical synthesis and rapid consolidation of a nanocrystalline 3.3Fe0.6Cr0.3Al0.1–Al_2O_3 composite by high frequency induction heating, Journal of Alloys & Compounds 509(2) (2011) L7–L10.

[16] S. Shamsuddin, S.B. Jamaludin, Z. Hussain, Z.A. Ahmad, The effects of Al_2O_3 amount on the microstructure and properties of Fe-Cr matrix composites, Metallurgical and Materials Transactions A 41(13) (2010) 3452-3457.

[17] K. Lemster, T. Graule, T. Minghetti, C. Schelle, J. Kuebler, Mechanical and machining properties of X38CrMoV5-1/Al_2O_3 metal matrix composites and components, Materials Science and Engineering: A 420(1) (2006) 296-305.

[18] C. Xuan, H. Shibata, S. Sukenaga, P.G. Jönsson, K. Nakajima, Wettability of Al_2O_3, MgO and Ti_2O_3 by liquid iron and steel, Isij International 55(9) (2015) 1882-1890.

[19] S. Vasic, B. Grobéty, J. Kuebler, P. Kern, T. Graule, Experimental Models for Activtation Mechanism of Pressureless Infiltration in the Non-Wetting Steel-Alumina MMC System, Advanced Engineering Materials 10(5) (2008) 471–475.

[20] K. Lemster, T. Graule, J. Kuebler, Processing and microstructure of metal matrix composites prepared by pressureless Ti-activated infiltration using Fe-base and Ni-base alloys, Materials Science and Engineering: A 393(1) (2005) 229-238.

[21] E. Wang, Y. Yi, H. Xie, Y. Fan, Effects of Ni and TiN Coatings on the Alumina/Heat-Resistant Steel Interface Properties, Applied Composite Materials 13(1) (2006) 23-29.

[22] J. Feizabadi, J.V. Khaki, M.H. Sabzevar, M. Sharifitabar, S.A. Sani, Fabrication of in situ Al_2O_3 reinforced nanostructure 304 stainless steel matrix composite by self-propagating high temperature synthesis process, Materials & Design 84 (2015) 325-330.

[23] N. Travitzky, P. Kumar, K. Sandhage, R. Janssen, N. Claussen, Rapid synthesis of Al_2O_3 reinforced Fe–Cr–Ni composites, Materials Science and Engineering: A 344(1) (2003) 245-252.

[24] X.G. He, D.H. Lu, S.M. Chen, Y.C. Xiong, Preparation and Thermal Shock Properties of Al_2O_3p/40Cr Functionally Graded Composites Materials, Applied Mechanics & Materials 328(4) (2013) 901-905.

[25] G.B.V. Kumar, C.S.P. Rao, N. Selvaraj, Mechanical and Tribological Behavior of Particulate Reinforced Aluminum Metal Matrix Composites – a review, Journal of Minerals & Materials Characterization & Engineering 10(1) (2011) 59-91.

[26] M.R. Rosenberger, C.E. Schvezov, E. Forlerer, Wear of different aluminum matrix composites under conditions that generate a mechanically mixed layer, Wear 259(1) (2005) 590-601.

[27] A. Akdemir, R. Kuş, M. Şimşir, Impact toughness and microstructure of continuous steel wire-reinforced cast iron composite, Materials Science & Engineering A 516(1–2) (2009) 119-125.

[28] G. Miyamoto, J. Oh, K. Hono, T. Furuhara, T. Maki, Effect of partitioning of Mn and Si on the growth kinetics of cementite in tempered Fe–0.6 mass%C martensite, Acta materialia 55(15) (2007) 5027-5038.

[29] X. Xu, W. Xu, F.H. Ederveen, S.V.D. Zwaag, Design of low hardness abrasion resistant steels, Wear 301(1–2) (2013) 89-93.

[30] O.P. Modi, D.P. Mondal, B.K. Prasad, M. Singh, H.K. Khaira, Abrasive wear behaviour of a high carbon steel: effects of microstructure and experimental parameters and correlation with mechanical properties, Materials Science & Engineering A 343(343) (2003) 235-242.

[31] C. Zhang, H. Zhou, L. Liu, Laminar Fe-based amorphous composite coatings with enhanced bonding strength and impact resistance, Acta Materialia 72(7) (2014) 239-251.

[32] Y. Cheng, L. Bian, Y. Wang, F. Taheri, Influences of reinforcing particle and interface bonding strength on material properties of Mg/nano-particle composites, International Journal of Solids & Structures 51(18) (2014) 3168-3176.

[33] P. Shen, H. Fujii, K. Nogi, Wetting, adhesion and diffusion in Cu–Al/SiO_2 system at 1473 K, Scripta Materialia 52(12) (2005) 1259-1263.

[34] T. Laha, S. Kuchibhatla, S. Seal, W. Li, A. Agarwal, Interfacial phenomena in thermally sprayed multiwalled carbon nanotube reinforced aluminum nanocomposite, Acta Materialia 55(3) (2007) 1059-1066.

[35] R.E. Neuendorf, E. Saiz, A.P. Tomsia, R.O. Ritchie, Adhesion between biodegradable polymers and hydroxyapatite: Relevance to synthetic bone-like materials and tissue engineering scaffolds, Acta Biomaterialia 4(5) (2008) 1288-1296.

[36] S. Sawla, S. Das, Combined effect of reinforcement and heat treatment on the two body abrasive wear of aluminum alloy and aluminum particle composites, Wear 257(5-6) (2004) 555-561.

[37] C.S. Ramesh, R. Keshavamurthy, B.H. Channabasappa, A. Ahmed, Microstructure and mechanical properties of Ni–P coated Si_3N_4 reinforced Al6061 composites, Materials Science & Engineering A 502(1–2) (2009) 99-106.

[38] A.P. Harsha, U.S. Tewari, B. Venkatraman, Three-body abrasive wear behaviour of polyaryletherketone composites, Wear 254(7-8) (2003) 680-692.

[39] D.K. Dwivedi, Adhesive wear behaviour of cast aluminium–silicon alloys: Overview, Materials & Design 31(5) (2010) 2517-2531.

[40] D. Lu, Y. Jiang, R. Zhou, Wear performance of nano-Al_2O_3 particles and CNTs reinforced magnesium matrix composites by friction stir processing , Wear 305(1-2) (2013) 286-290.

[41] Z.C. Lu, M.Q. Zeng, J.Q. Xing, M. Zhu, Improving wear performance of CuSn 5 Bi 5 alloys through forming self-organized graphene/Bi nanocomposite tribolayer, Wear s 364–365 (2016) 122-129.

[42] E. Schlenther, H. Özcoban, H. Jelitto, M. Faller, G.A. Schneider, T. Graule, C.G. Aneziris, J. Kuebler, Fracture toughness and corrosion behaviour of infiltrated Al_2O_3|P–Steel composites, Materials Science & Engineering A 590 (2014) 132-139.

[43] E. Schlenther, C.G. Aneziris, T. Graule, J. Kuebler, Influence of microstructural features on the impact toughness of infiltrated Al_2O_3|P-steel composites, Materials Science & Engineering A 556 (2012) 751-757.